Inelastic neutron spectra of polyacrylonitrile-based carbon fibers

Z. E. Brubaker, A. Miskowiec, Y. Q. Cheng, L. Daemen, and J. L. Niedziela

Phys. Rev. Materials **6**, 013609 — Published 26 January 2022

DOI: 10.1103/PhysRevMaterials.6.013609

Inelastic Neutron Spectra of PAN-based Carbon Fibers

Z. E. Brubaker,* A. Miskowiec, Y. Q. Cheng, L. Daemen, and J. L. Niedziela†
Oak Ridge National Laboratory, Oak Ridge, TN 37831
(Dated: January 11, 2022)

We present the vibrational spectra of polyacrylonitrile-based carbon fibers collected using inelastic neutron scattering. We ascertain the behavior of a broad range of vibrational spectra that are optically silent, and demonstrate a direct connection between these modes and thermomechanical properties of the fibers. We show directionally dependent coupling of hydrogen in the carbon fiber matrix, which is directly linked to mechanical properties. Further, we show hydrogen preferentially couples to the midband of the vibrational spectrum, and that there are higher overall mode populations in the traditional Raman D–G intervalley region, suggesting involvement of these modes in tensile strength reduction and transport properties.

I. INTRODUCTION

With their high strength-to-weight ratio, carbon fibers are actively sought as replacements for steel in many industrial applications. Carbon fiber microstructure can be described as connected graphitic subunits interspersed with defects and voids from the manufacturing process[1,2]. Manufacture of high-performance carbon fibers involves polymerization of a carbon-laden precursor with additional comonomers to obtain polyacrylonitrile (PAN) fibers, which are then stabilized in oxygen up to 300 °C and carbonized/graphitized up to 3,000 °C, often resulting in turbostratic end products. Current state-of-the-art high tensile strength carbon fibers have strengths registering about 5 GPa, despite the theoretical limit being estimated as high as 70 GPa[3–7]. Improving the tensile strength is thought to be driven by a decrease in overall defect concentration of the materials, with the highest tensile strength being achieved in defect-free, perfectly aligned graphene sheets. Substantial effort has been poured into process optimization for given parameters, in particular optimization of precursors, tensioning during the production process, oxidation, and graphitization conditions, but conditions designed to improve overall graphitic alignment result in higher stiffness, lower strength fibers[4,5].

Raman spectroscopy has traditionally been carried out on carbon-bearing materials to quantify the microstructure and impact of defects on the material[8–19]. The first order Raman spectra of carbon comprises the region between about 1,100 and 1,800 cm^{-1} and shows dominant D1 and G peaks near 1,350 and 1,580 cm^{-1}, respectively. The G band is related to the sp^2 bonded carbon atoms and is due to the doubly degenerate E_{2g} peak at the Brillouin zone center, whereas the D1 band is defect related, arising from a complex interaction with the electron band structure near the K point[15]. Because of this coupling mechanism, the D1 peak is dispersive with incident energy[20]. Additional peaks have been reported in this region, including the D2, D3, and D4 peaks near 1,620, 1,500, and 1,100 cm^{-1}, respectively[21]. The Raman spectral parameters have been used to establish correlations with crystallite size, strain, and mechanical properties (e.g., see[10,17,22–27]), and we recently demonstrated that the mechanical properties are most closely related to the D1 spectral parameters[21].

Fourier transform infrared spectroscopy (FTIR) has also been used to study carbon fiber structural features, but FTIR is significantly more sensitive to commercial coatings (i.e., sizings) applied to carbon fibers, and reliable spectral information is relatively sparse for pure carbon fibers. This is in part because graphene is optically silent to FTIR, while graphite yields a relatively limited FTIR response[28,29]. The available reliable data of carbon fibers exhibits a number of weak, broad features in the 800–1,800 cm^{-1} range, the intensity of which are substantially dependent on the experimental configuration[30–32]. Other observations are available in the literature but deal directly with the functional groups made available by surface coatings or oxidative procedures.

Although optical vibrational spectroscopies are a powerful probe for microscopic surface chemical characterization of materials, they are governed by electronic state transitions that restrict access to certain vibrational modes via the electronic state transition selection rules, and thus are inferential for many studies of the lattice dynamics of carbon materials. Additionally, experimental information on the spectral properties of carbon fibers are severely limited below 400 cm^{-1} which is due to the required experimental effort to extend below this limit on standard benchtop equipment.

Time-of-flight thermal neutron scattering allows bulk interrogation of the structure and dynamics of materials across a wide range of length and time scales in the absence of selection rules governing other optical spectroscopies. The lattice information available to optical spectroscopies is generally limited to coherence information over relatively long distances (hundreds of unit cells) within a sample, but neutron scattering can probe inter-cell correlations. Further, neutrons do not strongly interact with materials, making them nonperturbative for sample structure interrogations.

Here we present inelastic neutron scattering (INS) spectra of carbon fibers using thermal neutrons, collected using the vibrational spectrometer VISION[33,34] at the Spallation Neutron Source at Oak Ridge National Laboratory. We probe the inelastic neutron spectrum of four commercially available PAN-based carbon fibers to investigate the vibrational dynamics of the bulk material in the absence of scattering selection rules from optical spectroscopies. We contrast these results against the values of the vibrational spectra of polycrystalline graphite[34] and available spectroscopic information for graphite from neutron[35,36] and inelastic x-ray scattering[37,38]. We present evidence of carbon–hydrogen substitutional defects that preferentially couple to the D–G intervalley region and observe a direct dependence of bulk thermomechanical

Sample	Mod. (GPa)	Str. (GPa)	κ_l (W/cm-K)	α (10^{-6})	ρ_e ($m\Omega - cm$)	ρ_l (g/m)	C_p (J/gm-K)
T700	230	4.90	9.4	-0.388	1.6	1.8	0.752
IM-7	276	5.65	5.4	-0.64	1.5	1.78	0.878
T1000	294	6.37	10.5	-0.6	1.4	1.8	0.752
IM-10	310	6.96	6.14	-0.7	1.3	1.79	0.88

TABLE I. Manufacturer-provided thermomechanical properties of fiber samples used in the experiment.

properties on hydrogen content.

II. EXPERIMENTAL DETAILS

Carbon fiber samples used in the study were high-performance fibers from Toray (T700, T1000) and Hexcel (IM-7, IM-10), all derived from polyacrylonitrile (PAN) precursors. The bulk moduli and tensile strengths of the fibers ranged from 230 to 310 GPa and from 4.9 to 6.96 GPa, respectively. Manufacturer-provided thermophysical and mechanical data are presented in Tab. I. Representative Raman spectra are shown in Fig. 1, and show a decreasing D1 peak position and a decrease in interband intensity with increasing fiber modulus.

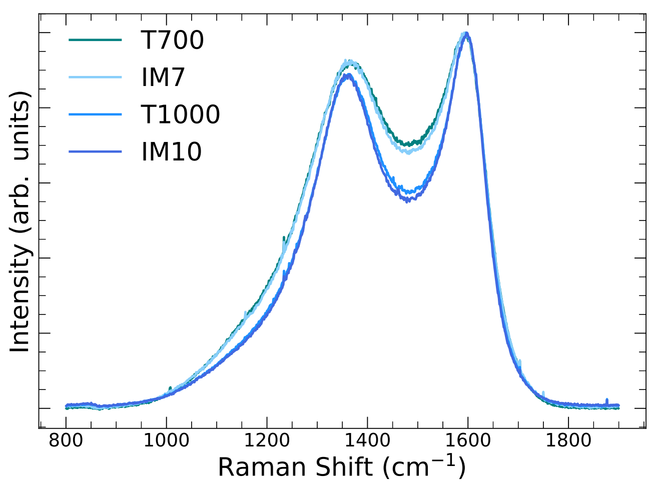

FIG. 1. Raman spectra of each carbon fiber acquired with a 100X objective and 532 nm excitation wavelength. The width and amplitude of the D1 peak near 1350 cm^{-1} decreases substantially with increasing modulus; see[21] for a more detailed discussion. The changes of the D1-peak may be correlated with hydrogen defects observed in the present work.

The IM-7, IM-10, and T-1000 fibers were all exposed to the neutron beam without removing the material sizing, while the T700 fiber was obtained from the manufacturer unsized. The sizing was not removed because the removal process involves volatile solvents and may leave hydrogenous residue on the sample surfaces that would complicate the measurement because of the strong incoherent neutron scattering cross section of hydrogen. Nonetheless, the material sizing appears to be of little consequence for the measured neutron scattering signal, likely because the sizing is only applied as a narrow surface layer and is thus an insignificant fraction of the total measured sample.

Fiber tows were wound (without twisting) onto 50 $\times$ 50 $\times$ 1 mm 6061 aluminum plates and were affixed with aluminum wire and overwrapped with aluminum foil. Fiber samples were then mounted in a closed cycle cryostat on the VISION spectrometer at the Spallation Neutron Source. VISION is a high-flux backscattering spectrometer capable of measuring vibrational spectra along two **Q** trajectories[33,39]. Here, we only show the results obtained from the high Q detector with Q = 2.2 Å^{-1} for the measured energy. In addition to the inelastic detectors, the instrument possesses diffraction detectors to measure static structure contributions.

As neutron scattering samples different portions of the phonon band structure depending on the sample orientation relative to the neutron beam[40], we elected to use different orientations of the fibers to the incident beam to assess the effect of incident beam orientation on the sample scattering.

To first order, by using distinct orientations, we can distinguish contributions from axial and radial alignment of the graphitic subunits and sample dynamics from different portions of the crystal structure[34]. Although substantial amounts of disorder are present in the carbon fiber materials[3,4], the manufacture process employs a consistent tension along the fiber axis at all production points, which preferentially orients the graphitic units relative to the axis of the carbon fibers[1,4]. Thus, we proceed with the assumption of relative alignment of the graphitic units along the fiber axis.

The two scattering conditions examined were with the incident beam parallel to the plane normal of sample plate (denoted $\mathbf{k}_i^{\perp}$) and with the incident beam 75 degrees from the plane normal of the sample plate (denoted $\mathbf{k}_i^{75}$). The $\mathbf{k}_i^{75}$ configuration struck a balance between background and signal. The distinction between the experimental configurations is such that the $\mathbf{k}_i^{\perp}$ configuration is sampling the plane perpendicular to the graphitic planes, while the $\mathbf{k}_i^{75}$ configuration is sampling more in-plane of the carbon units. All scattering studies were conducted at 5 K to minimize contributions from thermal vibrations. Data sets on the T700 fiber were taken for reduced time at 300 K in both the $\mathbf{k}_i^{\perp}$ and $\mathbf{k}_i^{75}$ configuration.

III. RESULTS AND DISCUSSION

Figure 2 plots the raw neutron diffraction patterns, and the inset shows the background-subtracted data near 2 Å; the full background-subtracted spectrum is shown in the appendix. The aluminum peaks are of comparable intensity as the primary peaks resulting from the carbon fibers and the sharp peaks and dips in the background-subtracted data result from

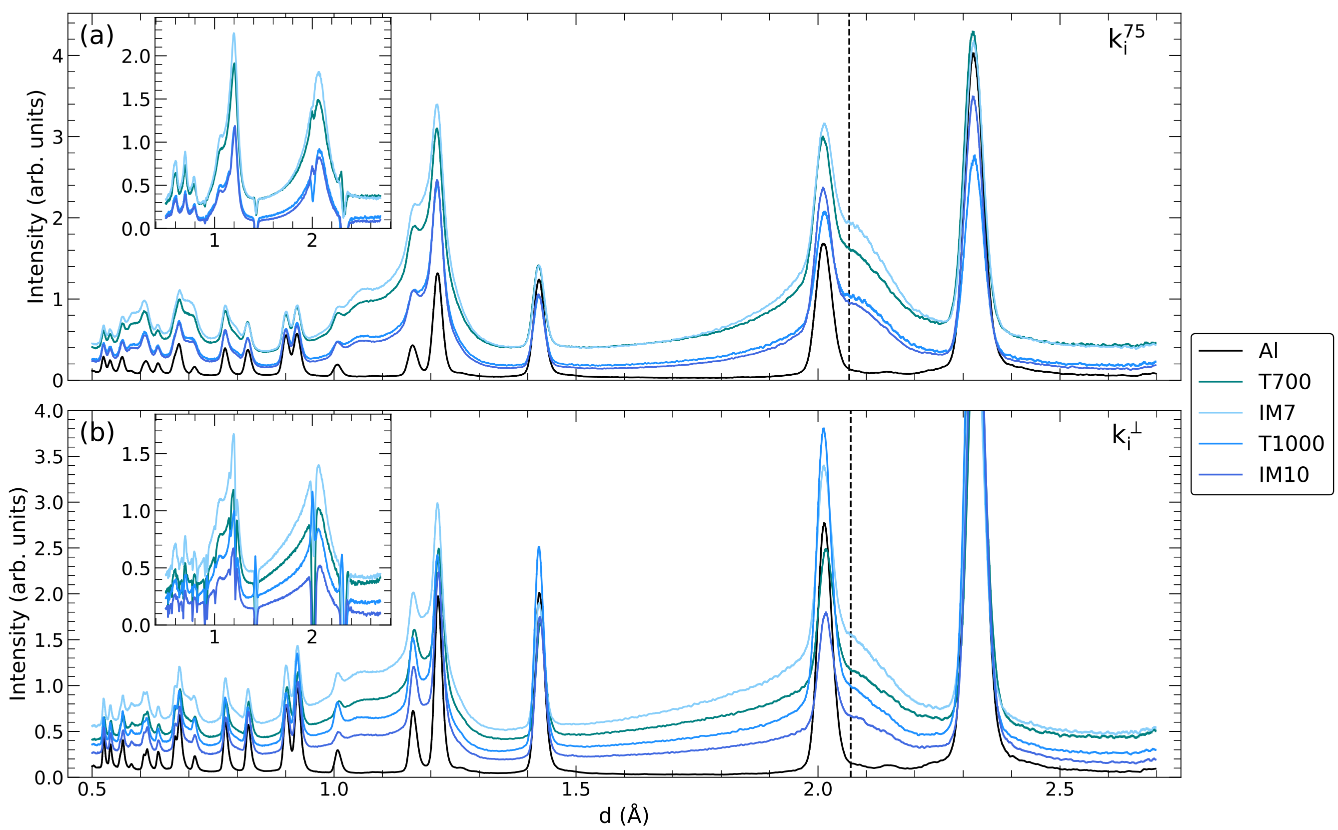

FIG. 2. Raw diffraction intensity overplotted with the background from the aluminum sample holder for the (a) $\mathbf{k}_i^{75}$ and (b) $\mathbf{k}_i^{\perp}$ configuration. The black dashed line shows the position of the peak that was used to normalize the inelastic neutron scattering data. Inset: background-subtracted data near 2 Å. All INS spectra were normalized to the peak height near 2 Å.

an imperfect background subtraction of the Bragg peaks of the aluminum mount. Given the substantial turbostratic disorder in the carbon fiber system, the peaks are quite broad, and a hybrid crystalline-amorphous character is seen to very low values of d. The peak near 2 Å is broadened considerably in the $\mathbf{k}_i^{\perp}$ configuration compared to $\mathbf{k}_i^{75}$ suggesting that larger crystallites are found in the out-of-plane direction of the carbon fibers. This observation is consistent with the general expectation that the crystallites are preferentially aligned along the fiber axis, likely due to the constant tension applied during manufacture. Unfortunately, the imperfect background subtraction, amorphous contributions and material texture preclude further quantitative analysis on the structural data.

Incident beam slits were used to reduce the size of the neutron beam to 30 $\times$ 30 mm. The total mass illuminated by the neutron beam is less than the total mounted mass ($\sim$1–3 g) and dependent on the effective size of the slit and the relative orientation of the beam and sample. To account for the distinct masses measured for each fiber and configuration, the presented INS data is normalized to the peak amplitude of the diffraction peak near 2 Å. The background near this peak was estimated from the average value from d = 2.5–2.6Å, and the peak height was selected as the maximum value near the peak. Although peak fitting would be preferable to extract the exact peak height, the background subtraction of the aluminum plate results in peaks that are poorly fit with traditional peak shapes.

Here, we are primarily concerned with the dynamical susceptibility, $\chi''(\mathbf{Q},E)$, which is a temperature-independent view of the system dynamics, removing effects from thermal population of the phonons. $\chi''(\mathbf{Q},E)$ is derived from the dynamical structure factor, $S(\mathbf{Q},E)$, following:

$$\chi''(\mathbf{Q},E) = (1-\exp(-\mathrm{E}/\mathrm{k_B T}))\mathrm{S}(\mathbf{Q},\mathrm{E}), \tag{1}$$

where E is the energy transfer, k_B is the Boltzmann constant, and T is the temperature of the measurement.

Results depicting $\chi''(\mathbf{Q},E)$ for all fibers at 5K are shown in Fig. 3. The background derived from the aluminum sample holder has been subtracted and the dominant contributions are only present up to the cutoff excitation energy for phonons in aluminum (40 meV, or 320 cm^{-1}). All data sets show a prominent feature near 100 cm^{-1}; this peak is an artifact from the experiment setup, but it also overlaps with the low energy optical mode of graphite[35,37].

First, we compare literature data collected on polycrystalline graphite[34] against the data from the carbon fibers. The data from polycrystalline graphite show substantive differences from the fiber materials, some of which may be due to the polycrystalline nature of the graphite powder versus

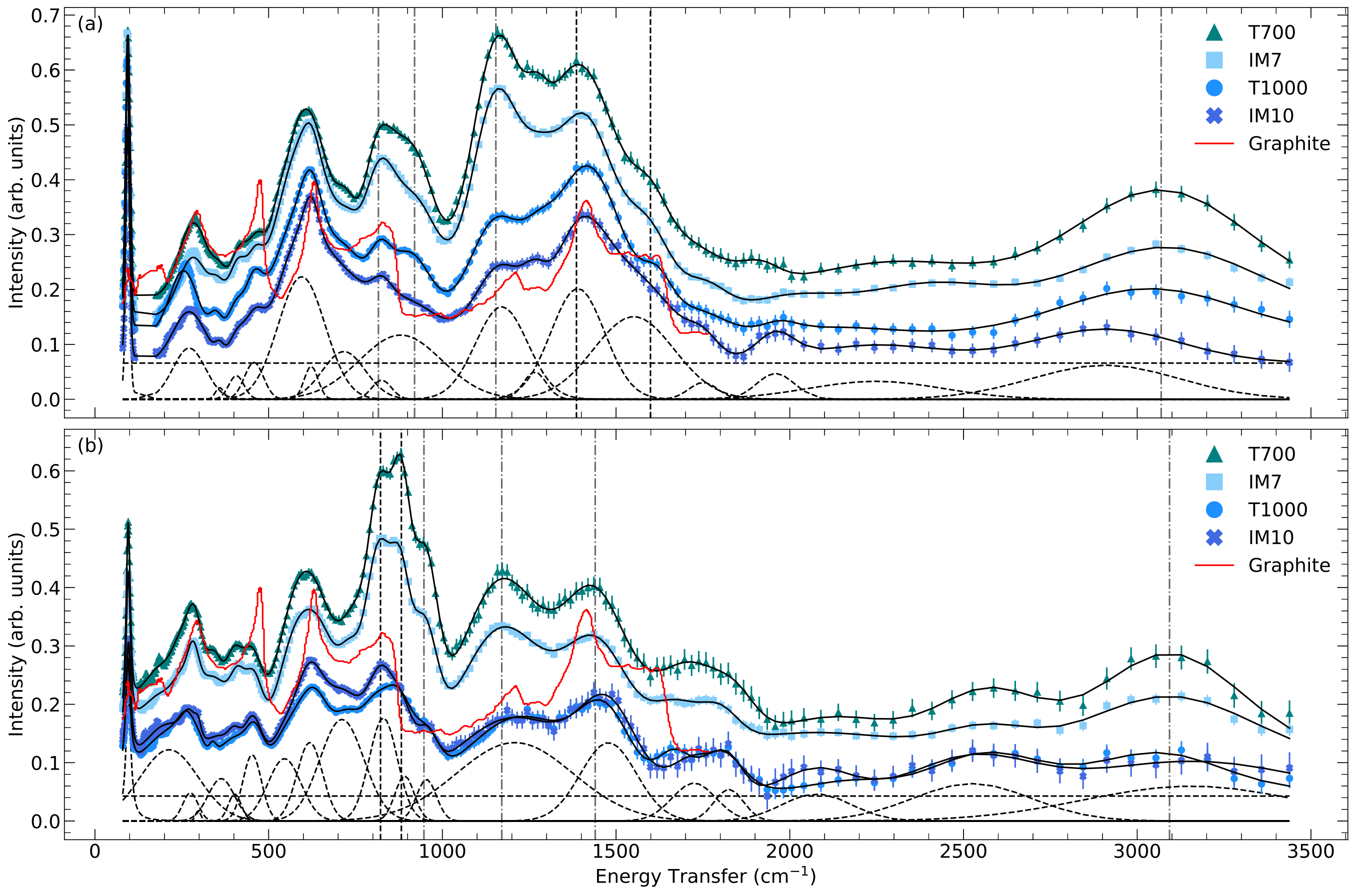

FIG. 3. INS spectra of carbon fibers collected in the (a) $\mathbf{k}_i^{75}$and (b) $\mathbf{k}_i^{\perp}$configurations. The data are background subtracted, corrected for the thermal occupation factor, and normalized to the diffraction peak near 2 Å. The constant background is not subtracted to highlight the incoherent scattering arising from hydrogen. The solid black lines correspond to the total fit for each spectrum and the dashed curves correspond to the fit components of the IM10 spectra. The vertical black dashed lines denote peaks discussed qualitatively, and the grey dot-dashed lines denote peaks discussed quantitatively in Fig. 4. The peaks highlighted near 800-900 cm^{-1} and 1200 cm^{-1} correspond to C–H bending modes. The solid red line corresponds to data obtained from polycrystalline graphite and is reproduced from[34].

the carbon fibers comprised of highly oriented graphitic units. The peak observed near 250 cm^{-1} corresponds to the transverse and longitudinal modes of the graphitic subunit and is seen in the graphite and carbon fiber data. However, the peak near 440 cm^{-1} is substantially diminished in the carbon fiber data. The intensity dip in the region near 550 cm^{-1} observed in graphite is preserved for the carbon fibers, but additional modes are observed in the intensity gap between 850 and 1,100 cm^{-1}. Additional differences are observed in the relative ratio of the peaks at 1,100 cm^{-1} to the peak near 1,500 cm^{-1}. Of note in both the graphite and the carbon fiber materials is the relative weakness of the peak near 1,580 cm^{-1} corresponding to the C–C stretching modes of the carbon nets. This peak is relatively constant in the graphite data, and of significantly reduced intensity in the fiber data.

Next, we compare the distinct carbon fibers. In both configurations, the modes in the region of 250–300 cm^{-1} are poorly fit with standard peak shapes; thus we decline to quantitatively discuss their widths or precise positions at this point. Qualitatively, the peak positions are higher in energy for the lower strength fibers, and the broadest distribution in the peak width is seen in the T700 fiber. Phonon linewidths are directly implicated in the thermal conduction mechanisms, with large contributions to overall phonon scattering mechanisms driving the overall lattice thermal conductivity[41]. Consequently, the behavior of these modes roughly tracks that shown in Tab. I.

Above 2,000 cm^{-1}, the spectra reveal a broad peak near 3,000 cm^{-1}. In carbon-based systems, peaks in this region correspond to C–H stretch modes, and based on previous works[29] we assign this mode as such. This peak is readily identified in all spectra and decreases in amplitude with increasing fiber modulus. In both configurations, this peak position shifts considerably for distinct fibers. Previous work on activated carbon fibers demonstrated that distinct C–H terminations result in distinct peak positions and intensities, which may explain the peak shifts observed in the present work[42].

The greatest distinctions in spectra between fibers is observed in the 800–1,800 cm^{-1} spectral region. In the $\mathbf{k}_i^{75}$ configuration, the two strongly overlapping peaks near 900 cm^{-1}, as well as the well-separated peaks near 1,200 and 1,400 cm^{-1}

are blunted with increasing fiber modulus. Additional peaks are observed in this region, though they do not show an obvious dependence on fiber type. In the $\mathbf{k}_i^{\perp}$ configuration, three strongly overlapping peaks between 800 and 950 cm^{-1} and two peaks near 1,200 and 1,500 cm^{-1} dominate the spectral region between 800 and 1,800 cm^{-1}. These peaks decrease in amplitude with increasing fiber strength, though the three peaks near 900 cm^{-1} are difficult to discern in the higher modulus fibers. For both configurations, the overall peak intensity near the 1,400 cm^{-1} peak likely arises from the K-point optical phonon mode[28,35,37], which is believed to be at least in part responsible for the *D* peak origin in the Raman measurements[14].

Several of the aforementioned peaks mirror the intensity dependence of the 3,000 cm^{-1} peak, suggesting that these may be C–H bending modes. Previous reports of activated carbons assigned the modes near 900 cm^{-1} to out-of-plane C–H bending modes, and the peak near 1200 cm^{-1} to in-plane C–H bending modes, and we assign these modes as such in the present work[43–47]. This assignment is consistent with the fact that these peaks are absent in polycrystalline graphite and is further supported by the fact that the out-of-plane modes near 900 cm^{-1} are much stronger in the $\mathbf{k}_i^{\perp}$ configuration, whereas the in-plane modes near 1200 cm^{-1} are much stronger in the $\mathbf{k}_i^{75}$ configuration. Additionally, previous work performed on activated carbons showed a similar triplet peak structure in the 800-950 cm^{-1} region, as observed in the $\mathbf{k}_i^{\perp}$ configuration in the present work[42,45–47]. Although some work has shown C–C modes in this region, we suggest that the peaks from 800-950 cm^{-1} and near 1,200 cm^{-1} most likely reflect C–H modes for each of the reasons listed above[?] . This assignment indicates preferential hydrogen coupling to modes active in the 800–1,800 cm^{-1} region, and consequently offers a plausible justification in the increase in D band intensity and D–G interpeak intensity observed in the Raman spectra for the lower strength fibers, as demonstrated in Figure 1. Interestingly, the flat background also varies with the C–H peak height near 3,000 cm^{-1}. This observation may imply that the baseline results from from multiple scattering events from hydrogen-based defects entrained in the carbon fiber.

To quantify the behavior of each configuration, we fit the data in the region between 70 and 3,500 cm^{-1} using a constant background, a pseudo-Voigt line shape for the peak near 100 cm^{-1} and Gaussian line shapes for the remaining peaks. The region between 115 and 175 cm^{-1} was excluded for the $\mathbf{k}_i^{75}$ fitting because one of the dominant aluminum background peaks appears in this region, and the background subtraction could not fully remove this artifact. A common set of peaks was chosen for each configuration, though the positions, widths, and amplitudes were allowed to vary within bounds. We use the fitting to establish quantitative correlations between select modes and thermomechanical properties. Note, owing to the number of peaks required to obtain a satisfactory fit, some of the spectral parameters show prohibitively large uncertainties. Here, we limit the discussion to peaks that yield small uncertainties in their spectral parameters and that show clear differences between fiber types. The selected peaks are marked in Fig. 3 with grey dot-dashed lines and correspond to C–H bending and stretching modes.

Figure 4 shows the selected peak amplitudes as a function of bulk modulus, tensile strength, and electrical conductivity for both configurations. In the case of the C–H stretch mode near 3,000 cm^{-1}, the peak amplitude decreases nearly linearly with increasing fiber modulus and fiber strength, and it increases linearly with increasing electrical conductivity for both configurations. Similar results are obtained for the constant background, which we attribute to incoherent hydrogen scattering. Because the $\mathbf{k}_i^{\perp}$ configuration is sampling the plane perpendicular to the graphitic planes, the linear relationship of the C–H amplitude to the mechanical properties demonstrated in the $\mathbf{k}_i^{\perp}$ data would suggest that remnant hydrogen in the interlayer spaces serve to suppress material strength and stiffness and facilitate higher electrical conductivity. The remaining peak amplitudes show similar qualitative changes with increasing modulus and highlight the strong hydrogen coupling observed in the 800–1,800 cm^{-1} spectral region.

IV. CONCLUSIONS

In summary, we have successfully used INS to measure the vibrational spectra from four varieties of PAN-based high tensile strength carbon fiber. We observe vibrational modes that cannot be seen with traditional optical spectroscopies down to 100 $cm^{-1}$and show that there are distinct contributions to the vibrational spectra between 800 and 1,800 cm^{-1}. We observe hydrogen scattering in the unsized fiber leading us to suggest significant hydrogen entrainment in the lower tensile strength carbon fibers. We show direct, directionally dependent coupling of hydrogen in the carbon fiber matrix and a strong linear connection between hydrogen content and thermo-mechanical properties. Enhancements of modes near 800-950 $cm^{-1}$and 1,200 cm^{-1} are particularly pronounced for lower tensile strength fibers, further supporting that increased crystalline coherency is disfavored for strength. The D–G interband valley intensity observed in Raman scattering is illustrated to be due to an increased overall density of modes that have preferential hydrogen coupling, which scale inversely with fiber strength and modulus.

This study used thermal neutron scattering to investigate the vibrational properties of carbon fibers using a broad energy range to elucidate underlying contributions to the vibrational properties of carbon fibers that have long been difficult to understand with Raman spectral data alone. Possible future work using neutrons to improve the state of understanding of the thermophysical properties of carbon fiber would include the use of cold neutrons to look at the mobility of the entrained hydrogen, and the dynamics of longer length scale objects in the carbon fiber matrix[48].

V. AUTHOR CONTRIBUTIONS

ZEB and JLN conducted experiments and analysis, AM contributed to experiment planning and data interpretation,

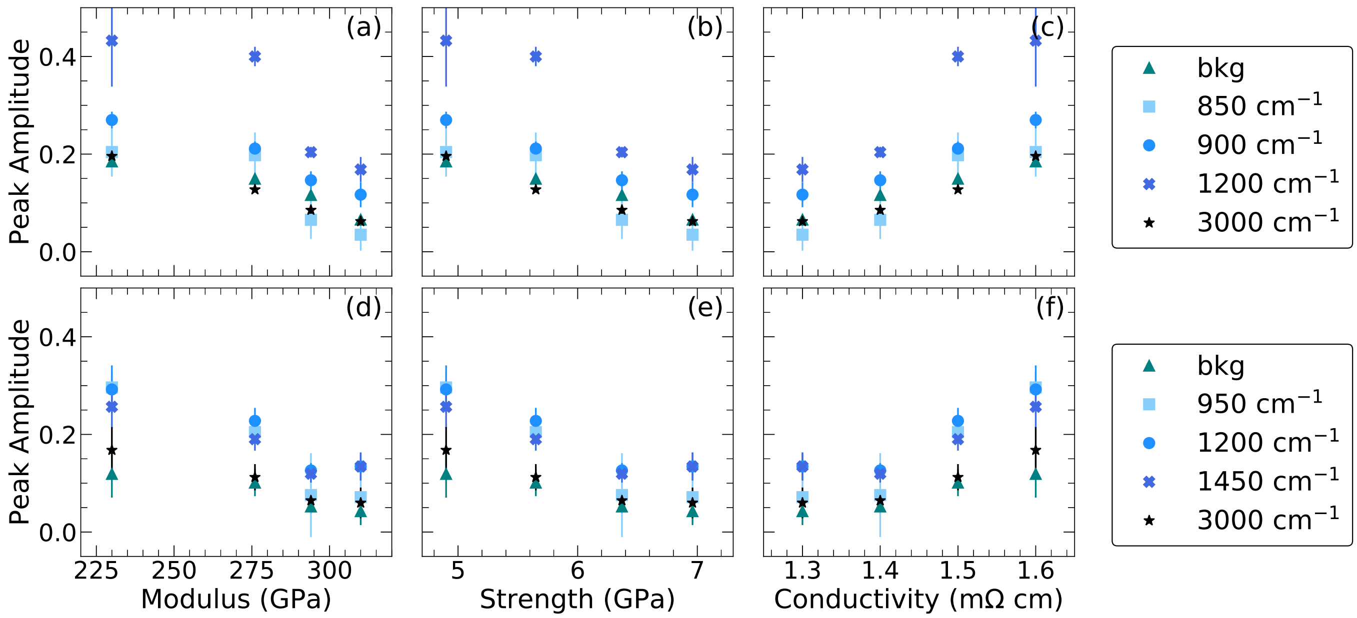

FIG. 4. Analysis of several peak amplitudes compared against thermomechanical properties for (a–c) $\mathbf{k}_i^{75}$ and (d–f) $\mathbf{k}_i^{\perp}$ configurations. The 3,000 cm^{-1} peak corresponds to the C–H stretch mode, and the background likely corresponds to incoherent scattering from hydrogen. The peak amplitude of the C–H stretch mode decreases with increasing modulus and strength and increases with increasing conductivity, suggesting that hydrogen-based defects critically affect the thermomechanical properties of fibers. Other peaks show similar trends and highlight strong coupling observed in the 800–1,800 cm^{-1} spectral region.

YQC and LD supported the experiment and data interpretation. ZEB and JLN wrote the manuscript with input from all authors. JLN supervised the project.

VI. ACKNOWLEDGMENTS

A portion of this research used resources at the Spallation Neutron Source, a Department of Energy Office of Science User Facility operated by the Oak Ridge National Laboratory. This research was funded by the US Department of Energy.

VII. APPENDIX

Figure 5 shows the background-subtracted neutron diffraction spectra. Substantial structure is noted in the diffraction pattern down to low d values. Unfortunately, the strong background peaks and imperfect background subtraction yield sharp dips and peaks that prohibit quantitative analysis of the diffraction patterns. Future work will improve the experimental setup to remove and suppress the background peaks.

As a last point, we compare the INS spectra of T700 fibers collected at 5 and 300 K in Fig. 6 for both configurations. Previous reports on thermal conductivity in carbon fibers observe orders of magnitude of difference in the thermal conductivity of fibers from 5 to 300 K[49,50], thus we expect to see distinctions between the 5 and 300 K spectra for the overall line shape of the phonon modes in the areas corresponding to the transverse and longitudinal modes. In addition to a broadening of the vibrational peaks, there is a definite downward shift of the mode near 200 cm^{-1}. We note that the data are presented as $\chi''(\mathbf{Q}, E)$, thus are corrected to account for thermal statistics.

* brubakerze@ornl.gov
† niedzielajl@ornl.gov

[1] B. A. Newcomb, Composites, A **91**, 262 (2016).
[2] D. Edie, Carbon **36**, 345 (1998).
[3] S. Chand, Journal of Materials Science **35**, 1303 (2000).
[4] E. Frank, L. M. Steudle, D. Ingildeev, J. M. Spörl, and M. R. Buchmeiser, Angewandte Chemie—International Edition **53**, 5262 (2014).
[5] R. Böhm, M. Thieme, D. Wohlfahrt, D. S. Wolz, B. Richter, and H. Jäger, Fibers **6** (2018).

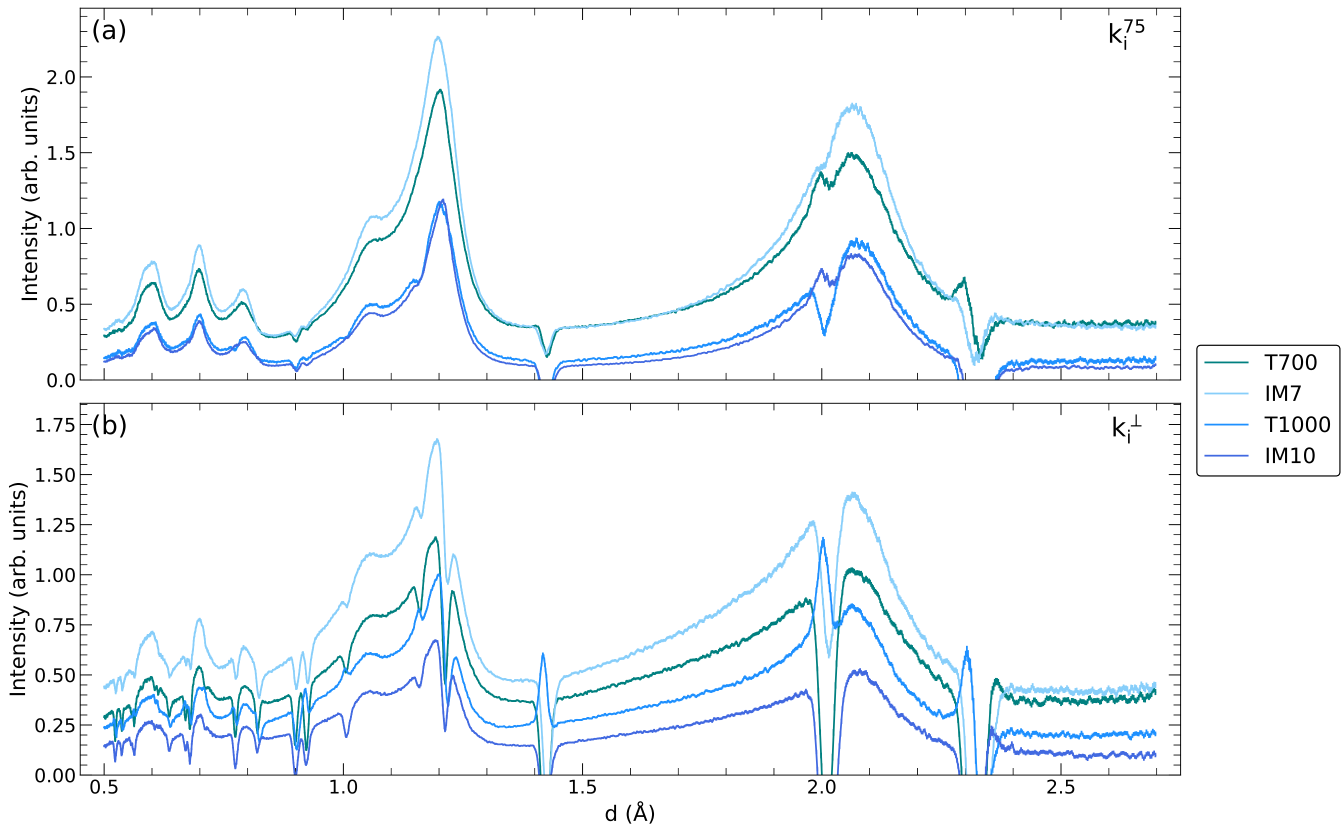

FIG. 5. Background subtracted data for all fibers from the (a) $\mathbf{k}_i^{75}$ and (b) $\mathbf{k}_i^{\perp}$ configuration. The relative positions of major crystallographic peaks are well aligned for the graphitic portions of the system. Substantial structural information is retained below d = 1Å. Sharp dips and spikes correspond to residuals from the background subtraction. All INS spectra were normalized to the peak height near 2 Å.

[6] H. G. Chae and S. Kumar, Science **319**, 908 (2008).
[7] D. C. Papageorgiou, I. A. Kinloch, and R. J. Young, Progress in Materials Science **90**, 75 (2017).
[8] F. Tuinstra and J. L. Koenig, Journal of Chemical Physics **53**, 1126 (1970), arXiv:arXiv:1011.1669v3.
[9] E. Fitzer and F. Rozploch, Carbon **26**, 594 (1988).
[10] N. Melanitis, P. L. Tetlow, and C. Galiotis, Journal of Materials Science **31**, 851 (1996).
[11] A. C. Ferrari and J. Robertson, Physical Review B **61**, 14095 (2000).
[12] L. G. Cançado, K. Takai, T. Enoki, M. Endo, Y. A. Kim, H. Mizusaki, A. Jorio, L. N. Coelho, R. Magalhães-Paniago, and M. A. Pimenta, Applied Physics Letters **88**, 1998 (2006).
[13] G. A. Zickler, B. Smarsly, N. Gierlinger, H. Peterlik, and O. Paris, Carbon **44**, 3239 (2006).
[14] A. C. Ferrari, Solid State Communications **143**, 47 (2007), arXiv:arXiv:0709.1174v1.
[15] M. J. Matthews, M. A. Pimenta, G. Dresselhaus, M. S. Dresselhaus, and M. Endo, Physical Review B **59**, R6585(R) (1999).
[16] A. C. Ferrari and D. M. Basko, Nature Nanotechnology **8**, 235 (2013), arXiv:1306.5856.
[17] H. Okuda, R. J. Young, F. Tanaka, J. Watanabe, and T. Okabe, Carbon **107**, 474 (2016).
[18] H. Okuda, R. J. Young, D. Wolverson, F. Tanaka, G. Yamamoto, and T. Okabe, Carbon **130**, 178 (2018).
[19] Y. Kaburagi, A. Yoshida, and Y. Hishiyama, *Materials Science and Engineering of Carbon—Characterization* (Elsevier, 2016).
[20] L. G. Cançado, A. Jorio, and M. A. Pimenta, Physical Review B **76**, 064304 (2007).
[21] Z. E. Brubaker, J. J. Langford, R. J. Kapsimalis, and J. L. Niedziela, Journal of Material Science , 1 (2021).
[22] Y. Huang and R. J. Young, J. Mater. Sci. **29**, 4027 (1994).
[23] O. Frank, G. Tsoukleri, I. Riaz, K. Papagelis, J. Parthenios, A. C. Ferrari, A. K. Geim, K. S. Novoselov, and C. Galiotis, Nature Communications **2**, 255 (2011).
[24] I. M. Robinson, M. Zakikhani, R. J. Day, R. Young, and C. Galiotis, Journal of Materials Science Letters **6**, 1212 (1987).
[25] H. Sakata, G. Dresselhaus, M. S. Dresselhaus, and M. Endo, Journal of Applied Physics **63**, 2769 (1988).
[26] F. Tanaka, T. Okabe, H. Okuda, I. Kinloch, and R. Young, Journal of Materials Science **48**, 3 (2013).
[27] T. Kobayashi, K. Sumiya, Y. Fukuba, M. Fujie, T. Takahagi, and K. Tashiro, Carbon **49**, 1646 (2011).
[28] D. D. L. Chung, Journal of Materials Science **37**, 1475 (2002).
[29] V. Tucureanu, A. Matei, and A. M. Avram, Critical Reviews in Analytical Chemistry **46**, 502 (2016).
[30] T. Ohwaki and H. Ishida, Journal of Adhesion **52**, 167 (1995).
[31] T. Ohwaki and H. Ishida, Applied Spectroscopy **49**, 341 (1995).
[32] M. S. de Oliveira Jr., M. F. Diniz, L. Dutra, Rita de Cassia, M. Massi, and C. Otani, Journal of Aerospace Technology and Management **8**, 26 (2016).
[33] S. F. Parker, A. J. Ramirez-Cuesta, and L. Daemen, Spectrochimica Acta Part A **190**, 518 (2018).
[34] Y. Q. Cheng, L. L. Daemen, A. I. Kolesnikov, and A. J. Ramirez-

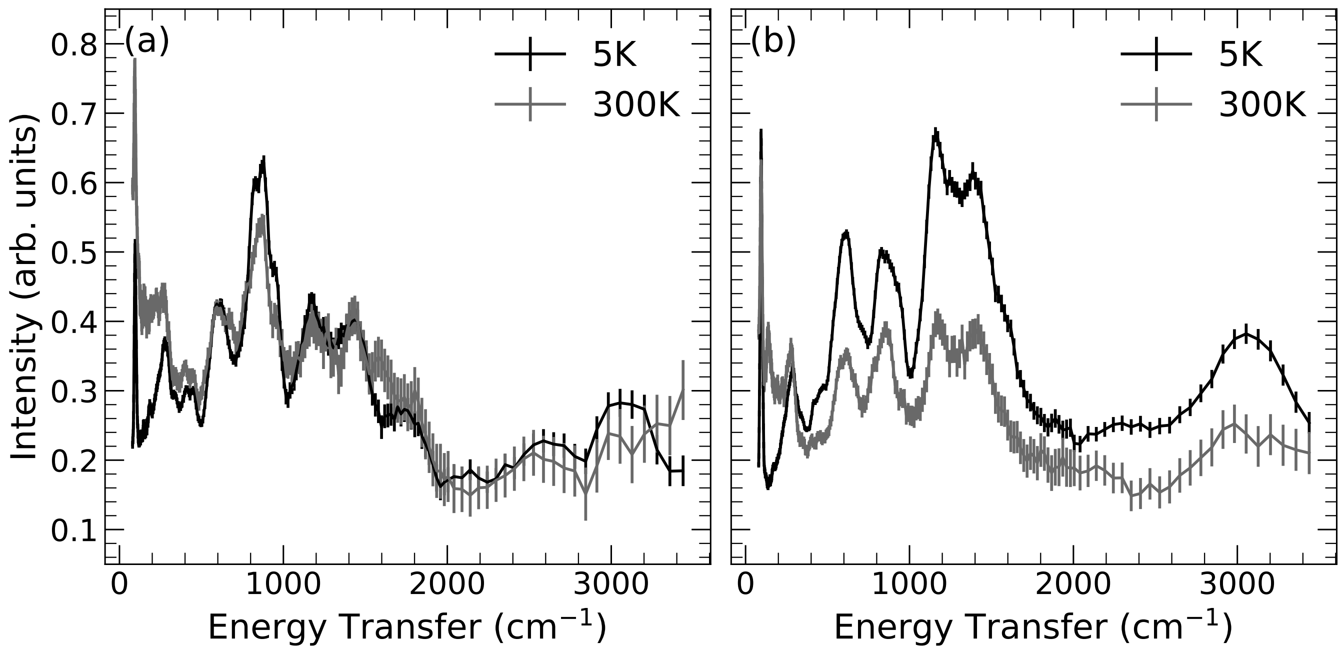

FIG. 6. INS spectra of T700 fibers at 5 K (black) and 300 K (grey) in the (a) $\mathbf{k}_i^{\perp}$ and (b) $\mathbf{k}_i^{75}$ configurations. Data at 300 K were acquired for less total time, resulting in a poorer counting statistic. The intensity mismatch is possibly due to a background subtraction issue, so we focus on the relative peak locations and shapes. The low energy acoustic band is broadened, and a new low energy peak appears in the $\mathbf{k}_i^{75}$ configuration near 120 cm^{-1}. The peaks near 800 cm^{-1} appear to merge, and ratio of peak intensities for the high energy peaks shifts.

Cuesta, Journal of Chemical Theory and Computation **15**, 1974 (2019), pMID: 30735379.

[35] R. Nicklow, N. Wakabayashi, and H. G. Smith, Physical Review B **5**, 4951 (1972).

[36] A. Burian, J. C. Dore, and K. Jurkiewicz, Reports on Progress in Physics **82**, 016501 (2019).

[37] J. Maultzsch, S. Reich, C. Thomsen, H. Requardt, and P. Ordejon, Physical Review Letters **92**, 075501 (2004).

[38] M. Mohr, J. Maultzch, E. Dobardszic, S. Reich, I. Milosevic, M. Damnjanovic, A. Bosak, M. Krisch, and C. Thomsen, Physical Review B **76**, 035439 (2007).

[39] P. A. Seeger, L. L. Daemen, and J. Z. Larese, Nuclear Instruments and Methods in Physics Research Section A **604**, 719 (2009).

[40] G. L. Squires, *Introduction to the Theory of Thermal Neutron Scattering*, 3rd ed. (Cambridge University Press, Cambridge, 2009).

[41] B. Fultz, Progress in Materials Science **55**, 247 (2010).

[42] E. Vottero, M. Carosso, M. Jiménez-Ruiz, R. Pellegrini, E. Groppo, and A. Piovano, Carbon **169**, 357 (2020).

[43] P. W. Albers, J. Pietsch, J. Krauter, and S. F. Parker, Phys. Chem. Chem. Phys. **5**, 1941 (2003).

[44] P. Albers, W. Weber, K. Möbus, S. Wieland, and S. Parker, Carbon **109**, 239 (2016).

[45] A. Piovano, A. Lazzarini, R. Pellegrini, G. Leofanti, G. Agostini, S. Rudić, A. L. Bugaev, C. Lamberti, and E. Groppo, Advances in Condensed Matter Physics **2015**, 803267 (2015).

[46] A. Lazzarini, A. Piovano, R. Pellegrini, G. Leofanti, G. Agostini, S. Rudić, M. R. Chierotti, R. Gobetto, A. Battiato, G. Spoto, A. Zecchina, C. Lamberti, and E. Groppo, Catal. Sci. Technol. **6**, 4910 (2016).

[47] A. Lazzarini, A. Piovano, R. Pellegrini, G. Agostini, S. Rudić, C. Lamberti, and E. Groppo, Physics Procedia **85**, 20 (2016).

[48] J. Cambedouzou, S. Rols, R. Almairac, J.-L. Sauvajol, H. Kataura, and H. Schober, Phys. Rev. B **71**, 041403 (2005).

[49] J. Heremans, I. Rahim, and M. S. Dresselhaus, Physical Review B **32**, 6742 (1985).

[50] J. Heremans and C. P. Beetz Jr., Physical Review B **32**, 1981 (1985).